Applied Catalysis B: Environmental 96 (2010) 41–50

Contents lists available at ScienceDirect

Applied Catalysis B: Environmental

journal homepage: www.elsevier.com/locate/apcatb

The effect of the crystalline phase of alumina on the selective CO oxidation in a hydrogen-rich stream over Ru/Al_2O_3

Yun Ha Kim, Eun Duck Park *

Division of Energy Systems Research and Division of Chemical Engineering and Materials Engineering, Ajou University, San 5, Woncheon-dong, Yeongtong-gu, Suwon, Kyunggi-do 443-749, Republic of Korea

ARTICLE INFO

Article history:
Received 3 December 2009
Received in revised form 22 December 2009
Accepted 1 February 2010
Available online 6 February 2010

Keywords:
Selective CO oxidation
PROX
Ru catalysts
PEMFC
Fuel cell

ABSTRACT

We prepared Ru catalysts supported on various aluminum oxides with different crystalline phases, viz. α-Al_2O_3, κ-Al_2O_3, γ-Al_2O_3, η-Al_2O_3, δ-Al_2O_3 and θ-Al_2O_3, by the incipient wetness method and applied them to the selective CO oxidation in a hydrogen-rich stream. For comparison, the complete CO oxidation in the absence of H_2 was also carried out over the same catalysts. Ru/α-Al_2O_3 showed the highest CO conversion among the tested catalysts, especially at low temperatures, irrespective of the presence of H_2. For all of the catalysts, the catalytic activity for CO oxidation was much suppressed in the absence of H_2 compared with that in the presence of H_2. Several techniques: N_2 physisorption, inductively coupled plasma-atomic emission spectroscopy (ICP-AES), X-ray diffraction (XRD), CO chemisorption, temperature-programmed oxidation (TPO), temperature-programmed reduction (TPR), temperature-programmed desorption (TPD) of CO_2 with mass spectroscopy and transmission electron microscopy (TEM) were employed to characterize the catalysts. The least amount of chemisorbed CO and CO_2 was obtained at room temperature over Ru/α-Al_2O_3. The least amount of O_2 was chemisorbed during TPO and the oxidized Ru species could be fully reduced in the presence of hydrogen at the lowest temperature over Ru/α-Al_2O_3 among the Ru/Al_2O_3 catalysts. Ru/α-Al_2O_3 can reduce a high inlet concentration of CO to less than 10 ppm even in the presence of H_2O and CO_2 over a wide temperature range.

1. Introduction

As concerns about energy and environmental problems increase, the interest in fuel cells, which can convert chemical energy directly into electricity, is increasing. Among the various types of fuel cell, polymer electrolyte membrane fuel cells (PEMFCs), which utilize H_2 as a fuel and can be operated at low temperatures, have recently attracted much attention because of their high power density and easy start-up [1]. On the other hand, they require rather complex fuel processing systems to meet the purity requirements of hydrogen in the present fossil fuel-based systems [2]. In the fuel processor for PEMFCs utilizing hydrocarbons as the raw fuel, a reformer, one or two shift reactors and CO removal units are generally installed. Unlike other high-temperature fuel cell systems such as phosphoric acid fuel cells (PAFCs), the CO present in hydrogen can degrade the electrochemical performance of the PEMFC severely even at ppm levels [2]. Therefore, it is generally recommended that the CO concentration should be reduced to less than 10 ppm [2,3]. Among the various ways to clean up CO in a hydrogen-rich stream, two representative catalytic reactions, preferential CO oxidation (PROX) and selective CO methanation, have been proposed [3]. In the PROX system, the following two reactions mainly occur:

$$CO + (1/2)O_2 \rightarrow CO_2, \quad (1)$$

$$H_2 + (1/2)O_2 \rightarrow H_2O, \quad (2)$$

In this case, it is necessary to identify the proper catalyst which can oxidize CO selectively in the presence of H_2 [3].

On the other hand, the following two hydrogenation reactions proceed during selective CO methanation:

$$CO + 3H_2 \rightarrow CH_4 + H_2O, \quad (3)$$

$$CO_2 + 4H_2 \rightarrow CH_4 + 2H_2O, \quad (4)$$

Therefore, an appropriate catalyst which is active for CO methanation is required. The above two hydrogenation reactions can also occur in the PROX system because all of the reactants (CO, CO_2 and H_2) are present simultaneously.

* Corresponding author. Tel.: +82 31 219 2384; fax: +82 31 219 1612.
E-mail address: edpark@ajou.ac.kr (E.D. Park).

0926-3373/$ – see front matter © 2010 Elsevier B.V. All rights reserved.
doi:10.1016/j.apcatb.2010.02.001

Until now, a number of catalysts have been reported for the PROX system [4–35]. These can be grouped into non-noble metal oxides [4–6], Au-based catalysts [4,7,8], Pt-based catalysts [4,9–18] and Ru-based catalysts [9,16–35]. Especially, Ru-based catalysts have been reported to be active for the PROX as well as the CO methanation reactions [36–42].

Based on comparisons of commercial noble metal catalysts for the PROX reaction, the Ru/Al_2O_3 catalyst has been proposed as the most active one [9,18]. In the case of Ru-based catalysts, the effect of various kinds of Ru precursors, the preparation methods, the pretreatment conditions and kinds of a support on the PROX activity have been examined. When supported Ru catalysts were prepared by the impregnation method, ruthenium nitrosylnitrate was reported to be the most adequate precursor among various precursors such as ruthenium chloride, ruthenium carbonyl and ruthenium nitrosylnitrate [19,20]. It was reported that the supported Ru catalyst directly reduced by H_2 showed higher PROX activity compared with those calcined in air and subsequently reduced in H_2 [20]. It was also proposed that additional pretreatment in a H_2/N_2 mixed gas flow could enhance the PROX activity of the Ru/Al_2O_3 catalyst [26].

In our previous work, we examined the effect of various supports on the PROX activity over supported Ru catalysts and proposed Ru/YSZ as the most active catalyst [33]. In the same work, $Ru/\gamma\text{-}Al_2O_3$ showed low catalytic activity [33]. Until now, $\gamma\text{-}Al_2O_3$ has been exclusively utilized as a support for the PROX reaction over Ru/Al_2O_3 catalysts [9,16–33]. For the same system, $\alpha\text{-}Al_2O_3$ has been claimed to be a promising support in a few patents [34,35]. To the best of our knowledge, no comparison work has been conducted for the PROX reaction over Ru catalysts supported on alumina with different crystalline phases and no relevant characterization has been conducted for $Ru/\alpha\text{-}Al_2O_3$ to explain its PROX activity.

In this work, we prepared various aluminum oxides with different crystalline phases to determine the effect of the crystalline phase of Al_2O_3 on the PROX activity over Ru/Al_2O_3 systematically.

2. Experimental

2.1. Support preparation

Various single-phase aluminum oxides were prepared through the thermal decomposition of bayerite, boehmite and gibbsite based on the procedure described in a previous work [43]. First, bayerite was prepared by the precipitation method. The pH of the aqueous solution of $Al(NO_3)_3{\cdot}9H_2O$ (Junsei Chem.) was increased to 10 by adding 1 M NH_4OH solution. The slurry was aged at 298 ± 2 K for 10 days, filtered and washed with distillated water. Then, the product was dried in air at 383 K for 1 day. Boehmite (Aldrich) and gibbsite (Samchun Chem.) were purchased and utilized. We prepared $\eta\text{-}Al_2O_3$ and $\theta\text{-}Al_2O_3$ through the calcination of bayerite at 873 K and 1273 K for 4 h, respectively. $\kappa\text{-}Al_2O_3$ was obtained after gibbsite was calcined at 1273 K for 4 h. We made $\delta\text{-}Al_2O_3$ through the calcination of boehmite at 1173 K.

2.2. Catalyst preparation

All of the catalysts were prepared by the incipient wetness method. $\alpha\text{-}Al_2O_3$ (Kanto) and $\gamma\text{-}Al_2O_3$ (Alfa) were purchased and utilized as a support. $\eta\text{-}Al_2O_3$, $\delta\text{-}Al_2O_3$, $\kappa\text{-}Al_2O_3$ and $\theta\text{-}Al_2O_3$ were prepared as described above and utilized as a support. Ruthenium nitrosylnitrate ($Ru(NO)(NO_3)_3{\cdot}xH_2O$, Aldrich) was utilized as a ruthenium precursor and the dried catalyst was reduced in a H_2 stream at 573 K without the calcination step. This catalyst preparation scheme has been proposed as the most effective procedure [20].

2.3. Catalyst characterization

The BET surface area was calculated from the N_2 adsorption data that were obtained using an Autosorb-1 apparatus (Quantachrome) at liquid N_2 temperature. Before the measurement, the sample was degassed in a vacuum for 4 h at 473 K. The results of the supports and catalysts are listed in Tables 1 and 2, respectively.

The Ru content of the prepared samples was analyzed by an inductively coupled plasma-atomic emission spectroscopy (ICP-AES, JY-70Plus, Jobin-Yvon). The results are displayed in Table 2.

The XRD patterns were recorded on a Rigaku D/MAC-III using Cu Kα radiation (λ = 0.15406 nm), operated at 40 kV and 100 mA (4.0 kW).

The pulsed chemisorptions of the probe molecules, viz. CO, CO_2 and O_2, were conducted in an AutoChem 2910 unit (Micromeritics) equipped with a thermal conductivity detector (TCD) to measure the consumption of each gas. Quartz U-tube reactors were generally loaded with 0.20 g of the sample except for $Ru/\alpha\text{-}Al_2O_3$. In the case of $Ru/\alpha\text{-}Al_2O_3$, 0.50 g of the sample was used. All of the catalysts were pretreated by reduction in H_2 at 573 K for 1 h, then cooled to room temperature. The chemisorptions were carried out at 300 K in a 30 ml/min stream of He using a pulsed-chemisorption technique, in which 500 l pulses of each gas were utilized. The results are listed in Table 1. Additionally, CO and O_2 chemisorptions were conducted over $Ru/\alpha\text{-}Al_2O_3$ at 373 K.

Temperature-programmed desorption (TPD) was conducted in an AutoChem 2910 unit (Micromeritics) equipped with a TCD and an on-line mass spectrometer (QMS 200, Pfeiffer Vacuum) to detect any organic or inorganic species in the effluent stream during the TPD experiment. Quartz U-tube reactors were generally loaded with 0.20 g of the sample. The TPD was performed after CO_2 chemisorptions using He with a flow rate of 30 ml/min in the temperature range from 313 K to 1173 K at a heating rate of 10 K/min after removing any weakly chemisorbed CO_2 in the line by flowing He at 313 K for 1 h.

Temperature-programmed oxidation (TPO) was conducted in an AutoChem 2910 unit (Micromeritics) equipped with a TCD to measure O_2 consumption. A water trap composed of blue silica gel was used to remove the moisture from the TPO effluent stream at 273 K before the TCD. Quartz U-tube reactors were generally loaded with 0.20 g of the sample, and the catalysts were pretreated by reductions with H_2 at 573 K for 1 h, then cooled to room temperature. The TPO was performed using 2 vol.% O_2/He with a flow rate of 30 ml/min in the temperature range from 313 K to 573 K at a heating rate of 10 K/min while monitoring the TCD signals after removing any residual hydrogen in the line by flowing He at 313 K for 1 h.

Temperature-programmed reduction (TPR) was conducted in an AutoChem 2910 unit (Micromeritics) equipped with a TCD to measure the H_2 consumption. A water trap composed of blue silica gel was used to remove the moisture from the TPR effluent stream

Table 1
The physicochemical properties of the alumina supports.

Supports	Surface area[a] (m^2/g)	Average pore diameter[b] (nm)	Pore volume[b] (cm^3/g)
$\alpha\text{-}Al_2O_3$	0.02	–	–
$\kappa\text{-}Al_2O_3$	32.3	38.2	0.29
$\gamma\text{-}Al_2O_3$	162.0	7.6	0.29
$\eta\text{-}Al_2O_3$	257.5	7.6	0.49
$\delta\text{-}Al_2O_3$	138.1	18.1	0.59
$\theta\text{-}Al_2O_3$	92.7	18.9	0.43

[a] The surface area was calculated by the BET method based on the N_2 physisorption data at liquid N_2 temperature.
[b] The average pore diameter and pore volume were calculated by the BJH method based on the N_2 desorption data at liquid N_2 temperature.

Table 2
The physicochemical properties of the supported Ru catalysts.

Catalyst	Ru content[a] (wt.%)	Surface area[b] (m^2/g)	Amount of chemisorbed CO[c] (μmol CO/$g_{cat.}$)	[CO]/[Ru][c]	Amount of chemisorbed CO_2[d] (μmol CO_2/$g_{cat.}$)	Amount of chemisorbed O_2 [e] (μmol O_2/g_{cat})	TPO peak area[f] (a.u.)	Amount of consumed H_2 [g] (μmol H_2/$g_{cat.}$)	$[H_2]/[Ru]$[h]
Ru/α-Al_2O_3	0.696	0.02	1.0	0.014	1.2	1.1	0.14	42.07	0.61
Ru/κ-Al_2O_3	0.694	27.5	9.9	0.14	8.4	0.6	0.33	100.08	1.46
Ru/γ-Al_2O_3	0.688	147.4	20.4	0.30	10.0	47.3	0.29	96.73	1.42
Ru/η-Al_2O_3	0.661	252.2	32.6	0.50	14.5	38.1	0.28	98.41	1.50
Ru/δ-Al_2O_3	0.673	106.5	26.0	0.39	14.1	35.7	0.27	93.74	1.41
Ru/θ-Al_2O_3	0.673	90.9	16.6	0.25	11.4	36.4	0.23	91.03	1.37

[a] The Ru content was determined by inductively coupled plasma-atomic emission spectroscopy (ICP-AES).
[b] The surface area was calculated by the BET method based on the N_2 physisorption data at liquid N_2 temperature.
[c] The CO chemisorptions were measured at 300 K in He.
[d] The CO_2 chemisorptions were measured at 300 K in He.
[e] The O_2 chemisorptions were measured at 300 K in He.
[f] The TPO peak area was calculated from the TPO pattern presented in Fig. 5.
[g] The amount of consumed H_2 during TPR after TPO was quantified based on the TPR of Ag_2O.
[h] The amount of consumed H_2 during TPR after TPO was normalized based on the amount of Ru in each catalyst.

at 273 K before the TCD. The reduction of Ag_2O was used to calibrate the TCD signal for the H_2 consumption. Quartz U-tube reactors were generally loaded with 0.20 g of the sample. The TPR was performed after TPO using 10 vol.% H_2/Ar with a flow rate of 30 ml/min in the temperature range from 313 K to 573 K at a heating rate of 10 K/min while monitoring the TCD signals after removing any residual oxygen in the line by flowing He at 313 K for 1 h.

Bright-field transmission electron microscopy (TEM) images were obtained using a Technai G^2 TEM (FEI) operated at 200 kV. The images were used to determine the particle size of Ru metal. The samples were ground in a mortar to fine particles and then dispersed ultrasonically in methanol. The sample was deposited on a Cu grid covered by a holey carbon film.

2.4. Reactor system and experimental procedure

The catalytic activity measurements were carried out in a small fixed bed reactor with catalysts that had been retained between 45 and 80 mesh sieves. For the screening tests, a standard gas consisting of 1 vol.% CO, 1 vol.% O_2 and 50 vol.% H_2 balanced with He was fed into the reactor, in which 0.10 g of the catalyst without diluents was brought into contact with the reactant gas at a flow rate of 100 ml (STP)/min, at atmospheric pressure. The catalytic activity was measured with a ramping rate of 0.33 K/min. For comparison, the complete CO oxidation in the absence of H_2 was also carried out over the same catalyst under the same condition except for the feed composition in which a standard gas consisting of 1 vol.% CO and 1 vol.% O_2 balanced with He was utilized.

In the case of Ru/α-Al_2O_3, the effect of the feed composition on the CO oxidation rate was measured in the differential reactor. In the differential reactor, 60 mg of Ru/α-Al_2O_3 were diluted with 440 mg of γ-Al_2O_3 and brought into contact with the reactant gas at a flow rate of 100 ml (STP)/min at 393 K at atmospheric pressure. The steady-state values were obtained for each condition.

For the Ru/α-Al_2O_3 catalyst, a realistic feed composition of 1 vol.% CO, 1 (or 0.5) vol.% O_2, 20 vol.% CO_2, 50 vol.% H_2, and 10 vol.% H_2O in He was adopted to confirm the catalytic performance. In this case, 0.50 g of the catalyst without diluents was brought into contact with the reactant gas at a flow rate of 50 ml (STP)/min at atmospheric pressure. The steady-state values were obtained at each temperature.

The effluent from the reactor was analyzed by a gas chromatography (HP5890A, carbosphere column) to determine the CO conversion, O_2 conversion, CO_2 selectivity and CH_4 yield. In all cases, the detection limit of CO was 10 ppm. The CO conversion, O_2 conversion, CO_2 selectivity and CH_4 yield were calculated using the following formulas:

$$\text{CO conversion } (\%) = \frac{[CO]_{in} - [CO]_{out}}{[CO]_{in}} \times 100,$$

$$O_2 \text{ conversion } (\%) = \frac{[O_2]_{in} - [O_2]_{out}}{[O_2]_{in}} \times 100,$$

$$CO_2 \text{ selectivity } (\%) = 0.5 \times \frac{[CO]_{in} - [CO]_{out}}{[O_2]_{in} - [O_2]_{out}} \times 100,$$

$$CH_4 \text{ yield } (\%) = \frac{[CH_4]_{out}}{[CO]_{in}} \times 100.$$

The CO_2 selectivity was reported only when CH_4 was not formed. A water trap was installed before the gas chromatography to remove all of the water vapor present in the feed or formed by the reactions.

3. Results and discussion

3.1. The physical properties of alumina

X-ray diffraction patterns were obtained for all of the supports used in this work to determine whether a single-phase aluminum oxide was developed for each support or not. As shown in Fig. 1, it was confirmed that each support has its own characteristic bulk crystalline structure [44]. It has been reported that γ-Al_2O_3 and η-Al_2O_3 have similar crystal structure and that η-Al_2O_3 has a sharper (1 1 1) peak than γ-Al_2O_3 [43], which is consistent with our results.

The adsorption and desorption isotherms of nitrogen were obtained for all of the supports to obtain some information on the surface area and pore size distribution. As shown in Fig. 2, a gradual increase in the volume of nitrogen adsorbed can be observed with increasing pressure of nitrogen relative to the saturated vapor pressure of nitrogen. As shown in Table 1, the pore volume increased in the following order: α-$Al_2O_3 \ll$ κ-$Al_2O_3 \approx$ γ-$Al_2O_3 <$ θ-$Al_2O_3 <$ η-$Al_2O_3 <$ δ-Al_2O_3. All of the supports except for α-Al_2O_3 exhibit hysteresis during the adsorption and desorption process. The pore size distribution was obtained from the desorption isotherm, as shown in Fig. 3. There is no noticeable peak corresponding to micro or mesopores for α-Al_2O_3. Table 1 shows that the average pore size increased in the following order: η-$Al_2O_3 \approx$ γ-$Al_2O_3 <$ δ-$Al_2O_3 <$ θ-$Al_2O_3 <$ κ-Al_2O_3. For all of the supports, no micropore volume can be measured by the *t*-plot method [45], which can be interpreted as meaning that only meso or macropores developed for all of the supports.

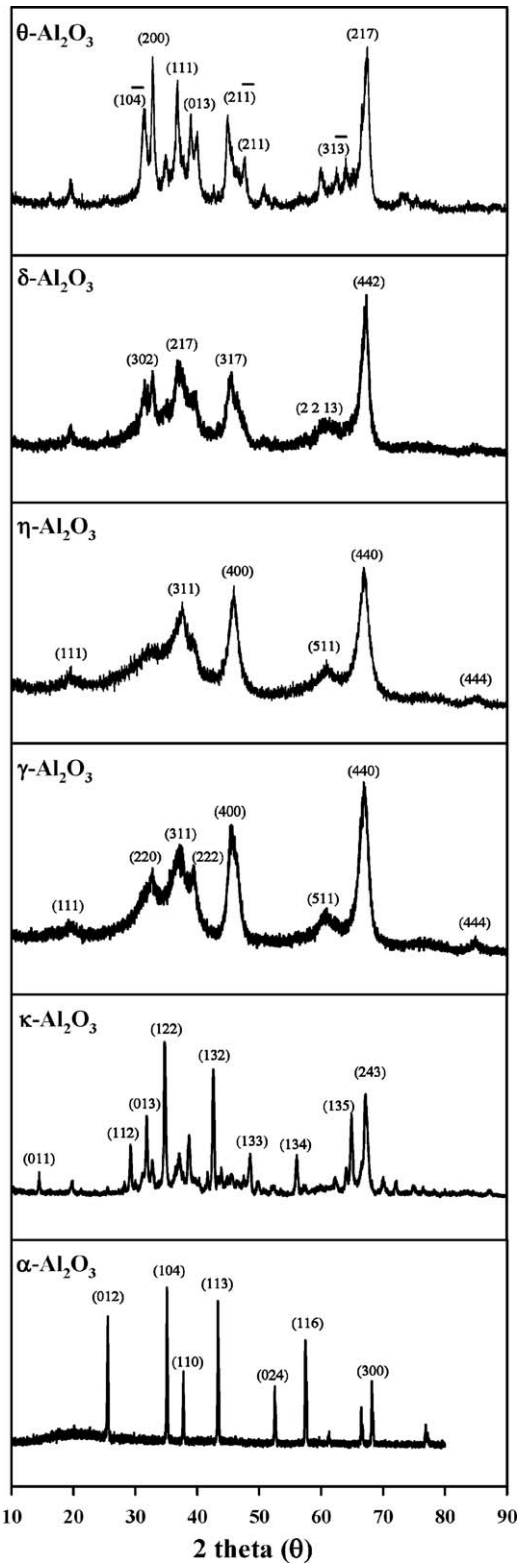

Fig. 1. X-ray diffraction patterns of various alumina supports, viz. α-Al_2O_3, κ-Al_2O_3, γ-Al_2O_3, η-Al_2O_3, δ-Al_2O_3 and θ-Al_2O_3.

3.2. Characterization of Ru/Al_2O_3 catalysts

Since CO and O_2 are main reactants for the PROX, CO and O_2 chemisorptions were performed for all of the supported Ru catalysts, as shown in Table 2. The amount of CO chemisorbed at 300 K decreased in the following order: Ru/η-Al_2O_3 > Ru/δ-Al_2O_3 > Ru/γ-Al_2O_3 > Ru/θ-Al_2O_3 > Ru/κ-Al_2O_3 ≫ Ru/α-Al_2O_3.

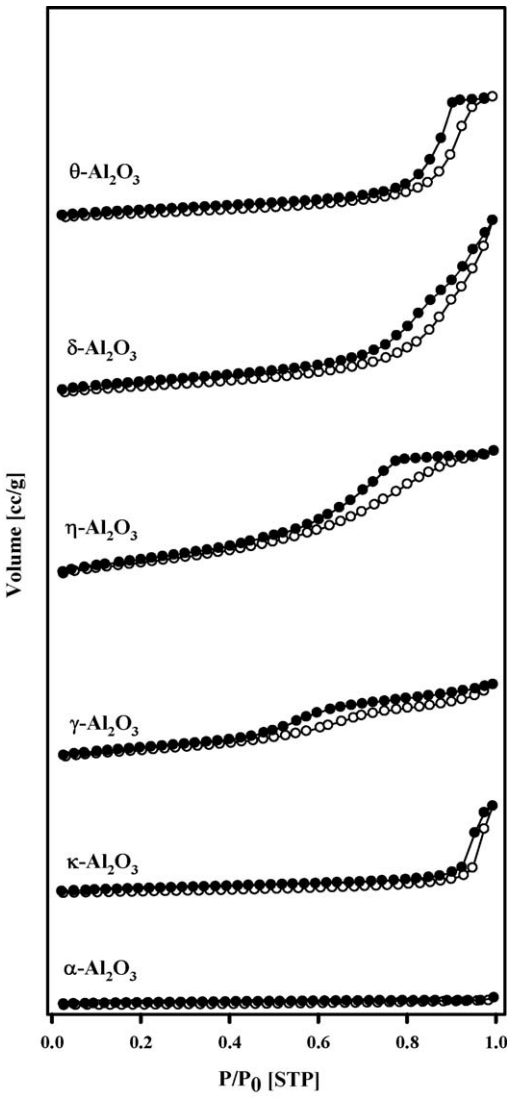

Fig. 2. Nitrogen adsorption (filled points) and desorption (unfilled points) isotherms of various alumina supports, viz. α-Al_2O_3, κ-Al_2O_3, γ-Al_2O_3, η-Al_2O_3, δ-Al_2O_3 and θ-Al_2O_3.

This order was maintained for the normalized amount of chemisorbed CO calculated based on the Ru content because all of the prepared catalysts have similar Ru contents. The amount of O_2 chemisorbed at 300 K decreased in the following order: Ru/γ-Al_2O_3 > Ru/η-Al_2O_3 > Ru/θ-Al_2O_3 ≈ Ru/δ-Al_2O_3 ≫ Ru/α-Al_2O_3 ≈ Ru/κ-Al_2O_3.

We also conducted CO_2 chemisorptions and the temperature-programmed desorption of CO_2 for all of the supported Ru catalysts. As listed in Table 2, the amount of CO_2 chemisorbed at 300 K decreased in the following order: Ru/η-Al_2O_3 > Ru/δ-Al_2O_3 > Ru/θ-Al_2O_3 > Ru/γ-Al_2O_3 > Ru/κ-Al_2O_3 ≫ Ru/α-Al_2O_3. As shown in Fig. 4, the CO_2-TPD peak maximum was observed at 365 K, 366 K, 373 K, 371 K and 367 K for Ru/κ-Al_2O_3, Ru/γ-Al_2O_3, Ru/η-Al_2O_3, Ru/δ-Al_2O_3 and Ru/θ-Al_2O_3, respectively. No noticeable CO_2-TPD peak can be found at low temperatures over Ru/α-Al_2O_3. On the other hand, the CO_2-TPD peak was also observed at high temperatures of around 650 K for all of the catalysts, which may be due to the strong interaction between the support and the chemisorbed CO_2.

Temperature-programmed oxidation (TPO) was carried out for all of the catalysts reduced in H_2 at 573 K to probe the different degrees of O_2 activation over the supported Ru catalysts, as shown

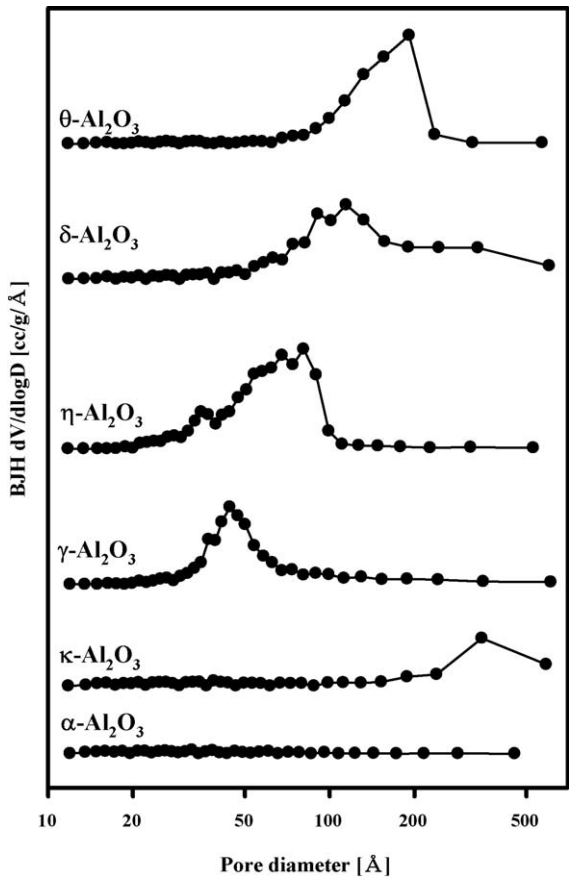

Fig. 3. Pore-size distribution plot for various alumina supports, viz. α-Al_2O_3, κ-Al_2O_3, γ-Al_2O_3, η-Al_2O_3, δ-Al_2O_3 and θ-Al_2O_3.

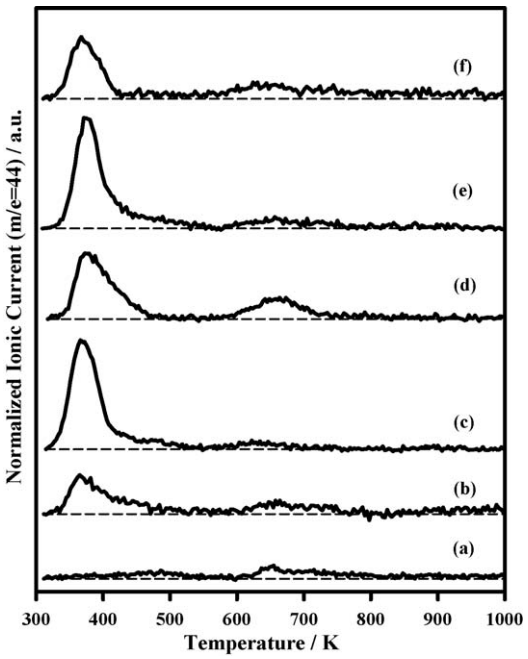

Fig. 4. The ionic current during the temperature-programmed desorption (TPD) for the supported Ru catalysts, viz. Ru/α-Al_2O_3 (a), Ru/κ-Al_2O_3 (b), Ru/γ-Al_2O_3 (c), Ru/η-Al_2O_3 (d), Ru/δ-Al_2O_3 (e) and Ru/θ-Al_2O_3 (f) after CO_2 adsorption at 300 K.

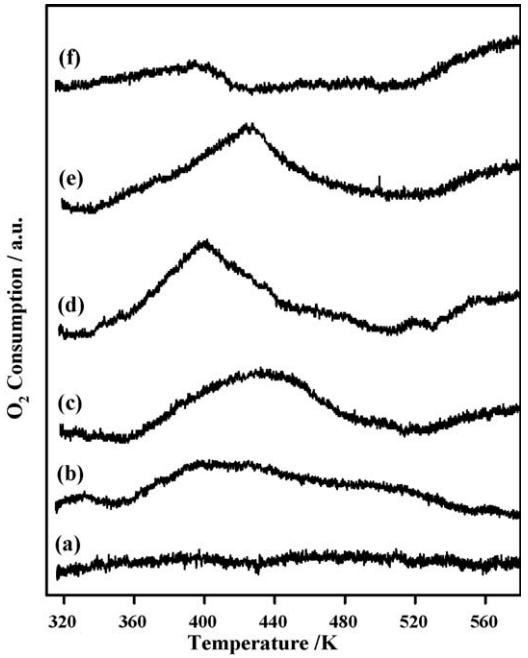

Fig. 5. The temperature-programmed oxidation (TPO) patterns of the supported Ru catalysts, viz. Ru/α-Al_2O_3 (a), Ru/κ-Al_2O_3 (b), Ru/γ-Al_2O_3 (c), Ru/η-Al_2O_3 (d), Ru/δ-Al_2O_3 (e) and Ru/θ-Al_2O_3 (f). All of the catalysts were reduced in H_2 at 573 K before the TPO experiment.

in Fig. 5. Ru/α-Al_2O_3 showed a very weak TPO peak from 320 K to 573 K, which implies that only small amount of O_2 was continuously consumed with increasing temperature. For all of the catalysts except for Ru/α-Al_2O_3, strong TPO peaks were obtained from 320 K to 573 K. A low-temperature TPO peak in the range from 320 K to 350 K and broad TPO peak in the range from 360 K to 570 K were observed over Ru/κ-Al_2O_3. A broad TPO peak was observed over Ru/γ-Al_2O_3 in the range from 360 K to 510 K. Rather sharp TPO peaks were observed over Ru/η-Al_2O_3 and Ru/δ-Al_2O_3 in the range from 330 K to 510 K. In the case of Ru/θ-Al_2O_3, a rather board TPO peak was obtained in the range from 320 K to 420 K but no consumption of O_2 was observed in the range from 420 K to 520 K. Since the TPO peak of volatile RuO_4 can appear at a much higher temperature than 573 K [46], all of the TPO peaks can be attributed to the oxidation of the chemisorbed H_2 and the bulk oxidation of metallic Ru into RuO_2 [47]. The TPO peak area which is directly related to the amount of O_2 consumed during the TPO experiment in the range from room temperature to 573 K was calculated for each catalyst, as shown in Table 2. Its value decreased in the following order: Ru/κ-Al_2O_3 > Ru/γ-Al_2O_3 ≈ Ru/η-Al_2O_3 ≈ Ru/δ-Al_2O_3 > Ru/θ-Al_2O_3 ≫ Ru/α-Al_2O_3.

Temperature-programmed reduction (TPR) was carried out after the TPO experiment to probe the reducibility of the oxidized Ru species, as presented in Fig. 6. It was previously reported that the H_2 consumption in the TPR profile can be ascribed to the reduction of Ru oxides [46]. The low-temperature peak can be ascribed to the reduction of well-dispersed RuO_2. On the other hand, the high-temperature peak can be assigned to the reduction of the bulky RuO_2 particles [47–53]. The TPR peak was observed in the range from 380 K to 420 K for Ru/α-Al_2O_3. The consumption of H_2 was observed starting from 320 K over Ru/κ-Al_2O_3, Ru/γ-Al_2O_3, Ru/η-Al_2O_3, Ru/δ-Al_2O_3 and Ru/θ-Al_2O_3. The amount of H_2 consumed during the TPR experiment was quantified, as listed in Table 2 and its value decreased in the following order: Ru/κ-Al_2O_3 > Ru/η-Al_2O_3 ∼ Ru/γ-Al_2O_3 > Ru/δ-Al_2O_3 > Ru/θ-Al_2O_3 ≫ Ru/α-Al_2O_3. This is in line with the relative amounts of O_2 consumed during the TPO experiment. The normalized amount of H_2 consumed during TPR based on the Ru content for each catalyst was calculated and its value is listed in Table 2. The Ru atom can be oxidized into RuO_2 ($Ru + O_2 \rightarrow RuO_2$) during TPO. In the TPR

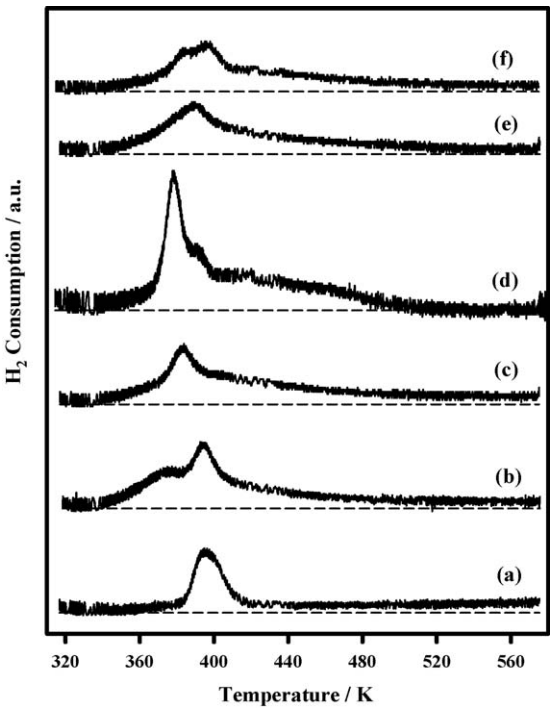

Fig. 6. The temperature-programmed reduction (TPR) patterns of the supported Ru catalysts, viz. Ru/α-Al_2O_3 (a), Ru/κ-Al_2O_3 (b), Ru/γ-Al_2O_3 (c), Ru/η-Al_2O_3 (d), Ru/δ-Al_2O_3 (e) and Ru/θ-Al_2O_3 (f) after the TPO experiment.

process, this oxidized Ru species can be reduced to metallic Ru ($RuO_2 + 2H_2 \rightarrow Ru + 2H_2O$). Therefore, the fraction of oxidized Ru atoms with respect to the total Ru atoms can be estimated to be a half of the [H_2]/[Ru] ratio listed in Table 2 for each catalyst.

To determine the particle size of Ru metals for all of the catalysts, TEM images were obtained in each case, as shown in Fig. 7. The average particle sizes of Ru metal in Ru/α-Al_2O_3, Ru/κ-Al_2O_3, Ru/η-Al_2O_3, Ru/δ-Al_2O_3 and Ru/θ-Al_2O_3 were determined to be 2.6 ± 0.6 nm, 9.1 ± 3.1 nm, 2.9 ± 1.0 nm, 4.0 ± 1.0 nm and 6.2 ± 1.5 nm, respectively. In the case of Ru/γ-Al_2O_3, the average particle size of Ru metal cannot be measured accurately. The average particle size of Ru metal for each catalyst decreased with increasing amount of chemisorbed CO presented in Table 2, except for Ru/α-Al_2O_3. In the case of Ru/α-Al_2O_3, all of the Ru metals appeared to be finely dispersed on the α-Al_2O_3 support and no agglomerated Ru particles could be found based on the TEM analysis. On the other hand, the amount of chemisorbed CO in Table 2 was much smaller than that estimated from the average particle size determined from the TEM images. Two different reasons can be proposed to explain the exceptionally small amounts of chemisorbed CO over the Ru/α-Al_2O_3. The first one is that the average particle size of Ru may be too large for it to chemisorb noticeable amounts of CO. However, this possibility can be excluded based on the TEM analysis. The other is that the electronic state of Ru metal can be modulated so as not to chemisorb CO properly at room temperature. This may be applicable to Ru/α-Al_2O_3 although further works are needed to support this proposal explicitly.

3.3. Comparison of the activity among the Ru/Al_2O_3 catalysts

The variation of the PROX activity with the reaction temperature over the supported Ru catalyst was examined in the integral reactor, as shown in Fig. 8. The catalytic activity for the preferential CO oxidation at low temperatures decreased in the following order: Ru/α-Al_2O_3 ≫ Ru/κ-Al_2O_3 ≫ Ru/γ-Al_2O_3 > Ru/η-Al_2O_3 > Ru/δ-Al_2O_3 ≈ Ru/θ-Al_2O_3. A high PROX activity, especially at low temperatures, is important for the PROX catalyst to be applied to small-scale fuel processor systems with their characteristic frequent on/off operation. During start-up and shut-down operation, the space velocity may become far less than that during steady-state operation, which can cause the amount of CO to be increased through the reverse water–gas shift reaction ($CO_2 + H_2 \leftrightarrow CO + H_2O$) over the PROX catalyst [15]. Because the reverse water–gas shift reaction is endothermic and thermodynamically limited, the equilibrium conversion decreases with decreasing temperature. Therefore, a PROX catalyst operating at low temperatures is desirable. The most active catalyst, Ru/α-Al_2O_3, has some advantageous characteristics. It can chemisorb the smallest amounts of CO and CO_2 among the tested catalysts. The amount of O_2 chemisorbed was much smaller at 300 K over this catalyst compared with the other supported Ru catalysts. Furthermore, the smallest amount of O_2 was consumed by this catalyst during the TPO experiment till 573 K. These results strongly support the view that the metallic Ru in Ru/α-Al_2O_3 cannot be oxidized easily compared with the other catalysts. Based on the result of the TPR after the TPO experiment, this catalyst can be fully reduced at the lowest temperature. It has been well accepted that the strong chemisorptions of CO is one of the reasons that supported Pt catalysts are not active for the PROX reaction at low temperatures [3,9]. Therefore, it is natural for Ru/α-Al_2O_3, having the smallest amount of chemisorbed CO, to show the highest PROX activity at low temperatures. We previously mentioned that their dominant and strong adsorption of CO_2 is one of the possible reasons for the low PROX activity over supported Ru catalysts [33]. It is meaningful to recall that the most active catalyst in this work, Ru/α-Al_2O_3, has the least amount of chemisorbed CO_2. In the case of Ru/α-Al_2O_3, the CO conversion increased rapidly at around 373 K, as shown in Fig. 8. We carried out the CO and O_2 chemisorptions for this catalyst at 373 K and found that the amount of CO chemisorbed was 2.7 μmol $CO/g_{cat.}$ which was far larger than that obtained at 300 K. On the other hand, a similar amount of O_2 was chemisorbed at 373 K to that measured at 300 K. Therefore, the rapid increase in the CO conversion must be due to the activated CO chemisorptions at this temperature.

Besides the PROX reaction, the CO methanation reaction also occurred at high temperatures and the temperatures, at which the formation of CH_4 was first observed, were 443 K for Ru/α-Al_2O_3, 473 K for Ru/κ-Al_2O_3, 513 K for Ru/γ-Al_2O_3 and Ru/δ-Al_2O_3, 523 K for Ru/θ-Al_2O_3 and 533 K for Ru/η-Al_2O_3. The CH_4 yield at 573 K decreased in the following order: Ru/δ-Al_2O_3 > Ru/θ-Al_2O_3 > Ru/κ-Al_2O_3 > Ru-/γ-Al_2O_3 > Ru/η-Al_2O_3 > Ru/α-Al_2O_3. Although the formation of methane can be observed over Ru/α-Al_2O_3 at the lowest temperature among the tested alumina-supported Ru catalysts, the CH_4 yield increased very slowly with increasing temperatures over this catalyst. It is noticeable that the formation of methane can be observed only after O_2 is completely consumed for all of the Ru catalysts. As mentioned in Section 1, the selective CO methanation can be one of the ways to remove CO in a H_2-rich stream. Therefore, the simultaneous PROX and CO methanation reactions can be considered to be plausible for supported Ru catalysts. However, a high Ru content and high reaction temperatures are required to achieve an acceptable level of CO removal through CO methanation only [40,41]. Because the conditions for the PROX reaction are not identical to those for the CO methanation reaction in most cases, the PROX catalyst with the lowest CO methanation activity would be desirable, so as not to consume additional H_2. From this view point, Ru/α-Al_2O_3 can be considered to be the most promising catalyst. The CO_2 selectivity decreased with increasing reaction temperature over the active catalysts, viz. Ru/α-Al_2O_3, Ru/κ-Al_2O_3, and Ru/γ-Al_2O_3, as shown in Fig. 8. On the other hand, the CO_2 selectivity showed a volcano plot as a function of the reaction temperature over Ru/δ-Al_2O_3,

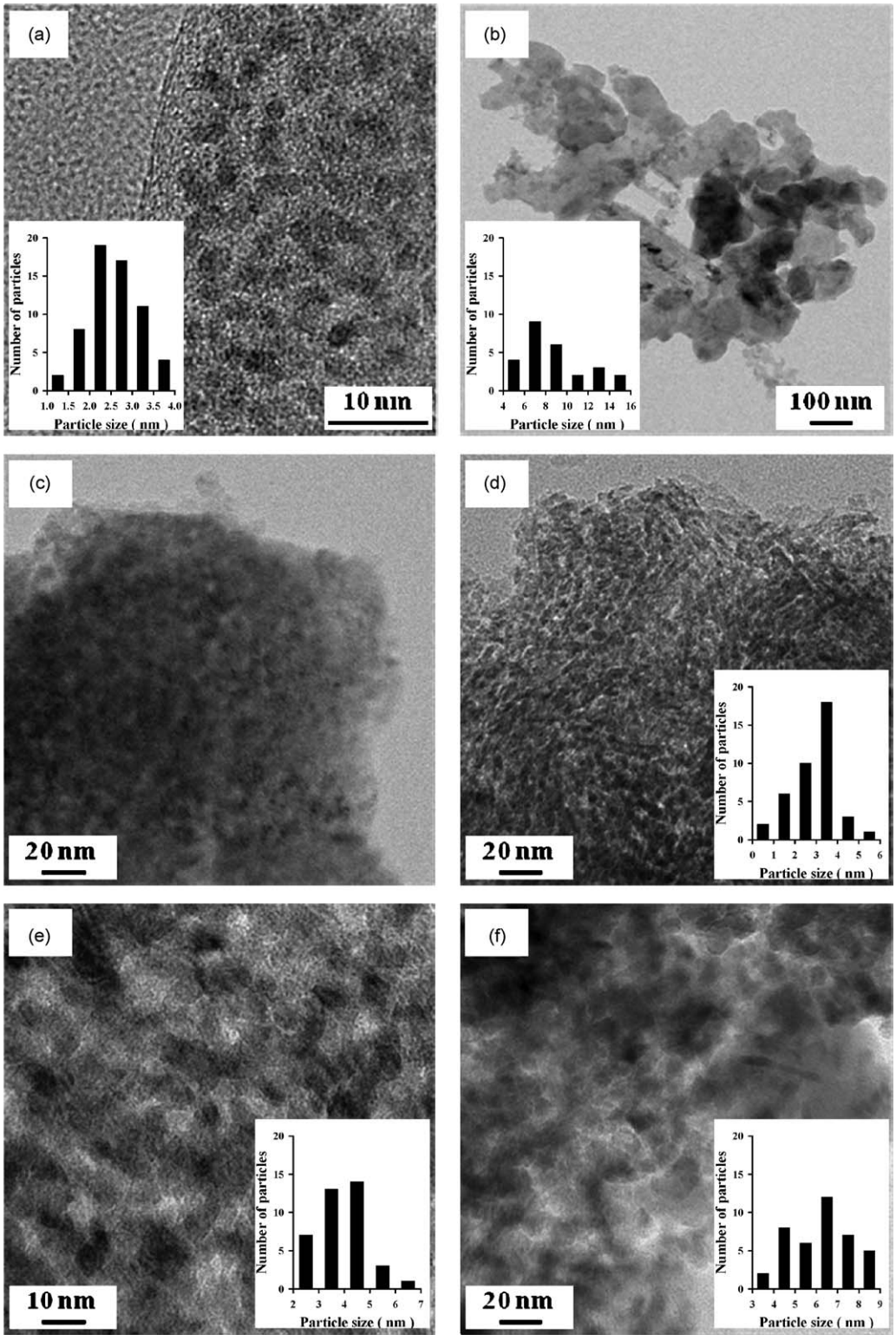

Fig. 7. The bright-field TEM images and particle size distributions of (a) Ru/α-Al_2O_3, (b) Ru/κ-Al_2O_3, (c) Ru/γ-Al_2O_3, (d) Ru/η-Al_2O_3, (e) Ru/δ-Al_2O_3 and (f) Ru/θ-Al_2O_3.

Ru/η-Al_2O_3, and Ru/θ-Al_2O_3 which exhibited noticeable PROX activity only at high temperatures. For these catalysts, metallic Ru can be transformed into RuO_2 as the reaction temperature is increased in the temperature region in which the O_2 conversion is low, as revealed by the TPO result. Therefore, the low CO_2 selectivity obtained over Ru/δ-Al_2O_3, Ru/η-Al_2O_3, and Ru/θ-Al_2O_3 may be due to the presence of oxidized Ru species. With further increasing reaction temperature, the CO_2 selectivity increased with increasing fraction of reduced Ru species in the presence of H_2 as described in the TPR result. The decreasing CO_2 selectivity with further increasing reaction temperature in the high temperature region can be explained by the predominant H_2 oxidation. The metallic Ru must be stable because all of the O_2 is consumed in this temperature region.

The CO oxidation activity in the absence of H_2 was also examined in the integral reactor over the supported Ru catalysts as

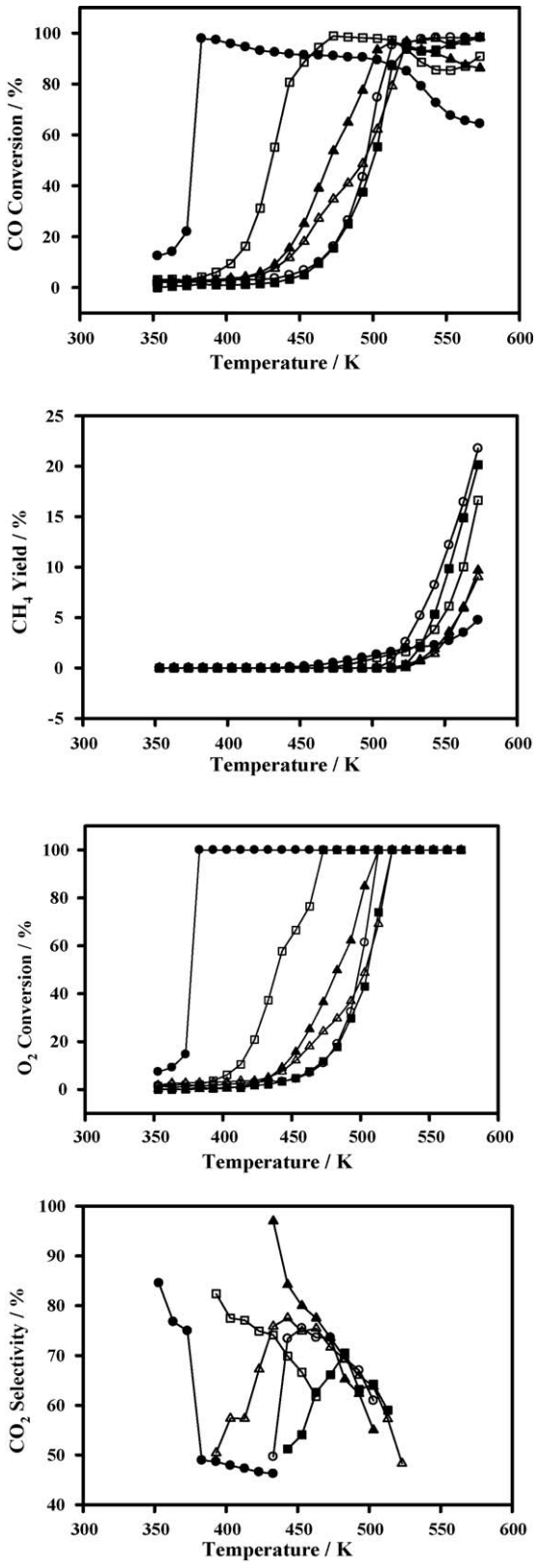

Fig. 8. Variation of the CO conversion, CH_4 yield, O_2 conversion and CO_2 selectivity for the selective CO oxidation with the reaction temperatures over the supported Ru catalysts, viz. Ru/α-Al_2O_3 (●), Ru/θ-Al_2O_3 (■), Ru/γ-Al_2O_3 (▲), Ru/δ-Al_2O_3 (○), Ru/κ-Al_2O_3 (□) and Ru/η-Al_2O_3 (△). F/W = 1000 ml/min/$g_{cat.}$. Reaction conditions: 1 vol.% CO, 1 vol.% O_2 and 50 vol.% H_2 in He.

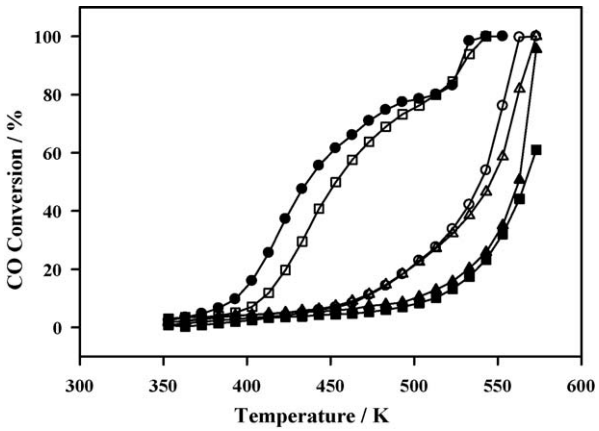

Fig. 9. Variation of the CO conversion for CO oxidation with the reaction temperatures over the supported Ru catalysts, viz. Ru/α-Al_2O_3 (●), Ru/θ-Al_2O_3 (■), Ru/γ-Al_2O_3 (▲), Ru/δ-Al_2O_3 (○), Ru/κ-Al_2O_3 (□) and Ru/η-Al_2O_3 (△). F/W = 1000 ml/min/$g_{cat.}$. Reaction conditions: 1 vol.% CO and 1 vol.% O_2 in He.

a function of the reaction temperature, as shown in Fig. 9. To compare the PROX activity, the same reaction conditions were adopted for this experiment except that there was no H_2 in the feed. The catalytic activity for the CO oxidation decreased in the following order: Ru/α-Al_2O_3 > Ru/κ-Al_2O_3 ≫ Ru/δ-Al_2O_3 > Ru/η-Al_2O_3 > Ru/γ-Al_2O_3 > Ru/θ-Al_2O_3. Compared with the PROX data, it was found that a similar CO conversion can be achieved at much higher temperature. As shown in the TPO patterns for all of the catalysts, O_2 was continually consumed starting from room temperature and was involved in the transformation of the metallic Ru into RuO_2. This activity data in the absence of H_2 strongly support the view that the metallic Ru is superior to the oxidized Ru species for CO oxidation. We reported that the preoxidized Ru/YSZ showed the much inferior PROX activity to the reduced one in our previous work [33]. Echigo and Tabata found that the additional pretreatment in a H_2/N_2 mixed gas flow could enhance the PROX activity of the Ru/Al_2O_3 catalyst [26]. These previous reports are in line with our present result.

Therefore, it is quite important to develop the supported Ru catalysts in which the metallic Ru is stable under PROX condition. From this view point, Ru/α-Al_2O_3 can be a promising catalyst because it can chemisorb the small amounts of O_2 at 300 K and it consumed the smallest amount of O_2 during the TPO experiment.

3.4. The catalytic performance over Ru/α-Al_2O_3

The effect of the feed composition for the PROX reaction over Ru/α-Al_2O_3 was investigated in the differential reactor at 393 K and is summarized in Table 3. Each experiment was conducted under reaction conditions in which no CH_4 was formed and stable catalytic activity was maintained. We found that the O_2 conversions in each experiment were similar to each other, even at the same contact time, which implies that there is no inhibition effect on the O_2 consumption rate, even in the presence of H_2O or CO_2. We kept the O_2 conversion low enough to achieve differential reactor conditions. The CO oxidation rate, as well as the CO_2 selectivity, decreased noticeably in the presence of H_2O or CO_2. This may be due to the competitive adsorption of H_2O and CO on the active sites. It should be noted that the O_2 consumption rate was not affected by the presence of H_2O or CO_2 in the feed. The strong adsorption of CO_2 on the catalyst surface, which was revealed in the CO_2-TPD results in Fig. 4, may be the reason for the lower CO oxidation rate in the presence of CO_2 in the feed. In all of the experiments, the initial CO oxidation rate and CO_2 selectivity were maintained. As shown in the TPO pattern in Fig. 5, the

Table 3
The catalytic performance over Ru/α-Al_2O_3 under different feed compositions at 393 K[a].

Feed composition	O_2 conversion (%)	CO oxidation rate (μmol CO s^{-1} $g_{cat.}^{-1}$)	CO conversion (%)	CO_2 selectivity (%)
1 vol.% CO, 1 vol.% O_2, and 50 vol.% H_2 in He	8.4	1.9	15.4	92 ± 2
1 vol.% CO, 1% O_2, 50 vol.% H_2, and 10 vol.% H_2O in He	8.2	0.9	7.5	46 ± 3
1 vol.% CO, 1 vol.% O_2, 50 vol.% H_2, and 20 vol.% CO_2 in He	8.2	0.8	6.7	41 ± 3
1 vol.% CO, 1 vol.% O_2, 50 vol.% H_2, 10 vol.% H_2O, and 20 vol.% CO_2 in He	8.4	0.9	7.5	45 ± 2

[a] The contact time was fixed at 12.4 μmol CO s^{-1} $g_{cat.}^{-1}$.

transformation of the metallic Ru into RuO_2 can occur during the reaction in the presence of O_2 over the supported Ru catalysts. On the other hand, the reduction of RuO_2 to metallic Ru can also occur during the PROX reaction in the presence of H_2, as revealed in Fig. 6. In the case of Ru/α-Al_2O_3, the least amount of O_2 was consumed during the TPO experiment and the oxidized Ru species could be reduced at the lowest temperature based on the TPR pattern after the TPO experiment. Therefore, we can say that the active metallic Ru can be preserved over α-Al_2O_3.

Until now, only a few studies have reported an exit concentration of CO from a catalytic CO removal unit of less than 10 ppm under realistic conditions. Although Echigo et al. [26–30] obtained acceptable PROX activity over Ru/Al_2O_3 under realistic condition, the CO concentration in the feed stream was rather low. Since Ru/α-Al_2O_3 can be considered to be the most promising catalyst in this work, the catalytic performance over Ru/α-Al_2O_3 was examined under realistic conditions, in which the feed was composed of 1.0 vol.% CO, 1.0 or 0.5 vol.% O_2, 20.0 vol.% CO_2, 50.0 vol.% H_2, and 10.0 vol.% H_2O in He, as shown in Fig. 10. In the case where λ (the ratio of O/CO) = 1, the CO conversion was about 80% from 383 K to 403 K. The CO_2 selectivity was also about 80% from 383 K to 403 K, because the O_2 conversions were 100%. Under the same conditions, the CH_4 yield was below 0.5% at 438 K. We increased the O_2 concentration for λ to 2 and obtained 100% CO conversion (i.e., an exit CO concentration of less than 10 ppm) from 383 K to 413 K. In the same temperature region, the CO_2 selectivity was about 50%. Under the same reaction conditions, the CH_4 yield was below 3% at 423 K. Compared with the cases with 5 wt.% Ru/γ-Al_2O_3 [18] and Ru/YSZ [33], the consumption of H_2 was not severe over Ru/α-Al_2O_3, which is more plausible.

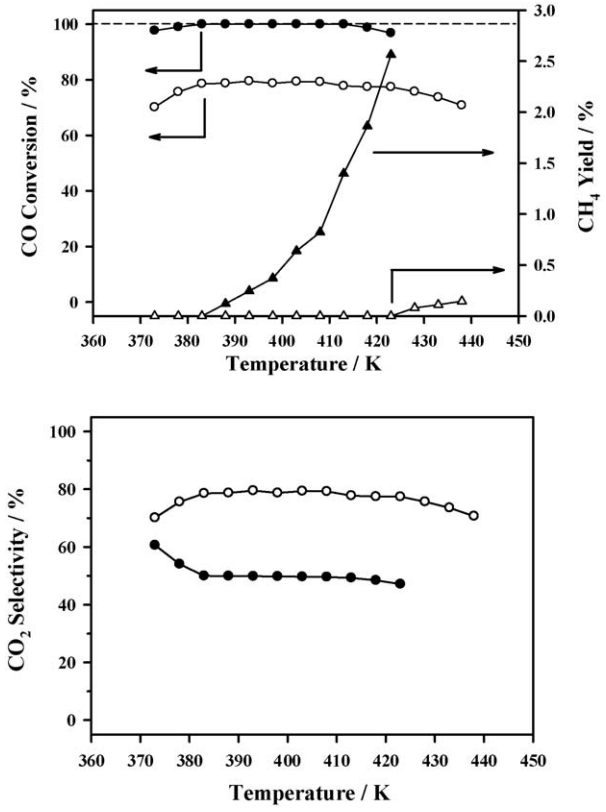

Fig. 10. The steady-state CO conversion, CH_4 yield and O_2 conversion for the PROX reaction over Ru/α-Al_2O_3 at different reaction temperatures. F/W = 50 ml/min/$g_{cat.}$. Reaction conditions: 1 vol.% CO, 1 vol.% O_2 (●, ▲) or 0.5 vol.% O_2 (○, △), 50 vol.% H_2, 20 vol.% CO_2 and 10 vol.% H_2O in He.

4. Conclusion

Irrespective of the presence of H_2, Ru/α-Al_2O_3 showed the highest CO conversion among the Ru catalysts supported on alumina with various single phases, viz. α-Al_2O_3, κ-Al_2O_3, γ-Al_2O_3, η-Al_2O_3, δ-Al_2O_3 and θ-Al_2O_3, especially at low temperatures. The least amount of chemisorbed CO and CO_2 was observed at room temperature over Ru/α-Al_2O_3. Among the Ru/Al_2O_3 catalysts, the least amount of O_2 chemisorbed during the temperature-programmed oxidation (TPO) experiment was observed over Ru/α-Al_2O_3 and the oxidized Ru species were fully reduced in the presence of hydrogen at the lowest temperature over this catalyst. The catalytic activity for CO oxidation was much suppressed in the absence of H_2 compared with that in the presence of H_2, which strongly supports the view that the metallic Ru is superior to the oxidized Ru species for CO oxidation. Ru/α-Al_2O_3 can reduce the high inlet CO concentration to less than 10 ppm even in the presence of H_2O and CO_2 over a wide temperature range.

Acknowledgements

This work was supported by Priority Research Centers Program through the National Research Foundation of Korea (NRF) funded by the Ministry of Education, Science and Technology (2009-0094047). This work was also supported by the Next Generation Military Battery Research Center program of Defense Acquisition Program Administration and Agency for Defense Development.

References

[1] C. Song, Catal. Today 77 (2002) 17–49.
[2] B.C.H. Steele, A. Heinzel, Nature 414 (2001) 345–352.
[3] E.D. Park, D. Lee, H.C. Lee, Catal. Today 139 (2009) 280–290.
[4] E.-Y. Ko, E.D. Park, K.W. Seo, H.C. Lee, D. Lee, S. Kim, Catal. Today 116 (2006) 377–383.
[5] D. Gamarra, C. Belver, M. Fernández-García, A. Martínez-Arias, J. Am. Chem. Soc. 129 (2007) 12064–12065.
[6] F. Mariño, C. Descorme, D. Duprez, Appl. Catal. B: Environ. 58 (2005) 175–183.
[7] W. Deng, J.D. Jesus, H. Saltsburg, M.F. Stephanopoulos, Appl. Catal. A: Gen. 291 (2005) 126–135.
[8] R.J.H. Grisel, B.E. Nieuwenhuys, J. Catal. 199 (2001) 48–59.
[9] S.H. Oh, R.M. Sinkevitch, J. Catal. 142 (1993) 254–262.
[10] C. Pedrero, T. Waku, E. Iglesia, J. Catal. 233 (2005) 242–255.
[11] M.M. Schubert, M.J. Kahlich, G. Feldmeyer, M. Hüttner, S. Hackenberg, H.A. Gasteiger, R.J. Behm, Phys. Chem. Chem. Phys. 3 (2001) 1123–1131.
[12] A. Fukuoka, J. Kimura, T. Oshio, Y. Sakamoto, M. Ichikawa, J. Am. Chem. Soc. 129 (2007) 10120–10125.
[13] E.-Y. Ko, E.D. Park, K.W. Seo, H.C. Lee, D. Lee, S. Kim, Angew. Chem. Int. Ed. 46 (2007) 734–737.
[14] F. Mariño, C. Descorme, D. Duprez, Appl. Catal. B: Environ. 54 (2004) 59–66.
[15] O. Korotkikh, R. Farrauto, Catal. Today 62 (2000) 249–254.

[16] H. Wakita, Y. Kani, K. Ukai, T. Tomizawa, T. Takeguchi, W. Ueda, Appl. Catal. A: Gen. 283 (2005) 53–61.
[17] Y.-F. Han, M.J. Kahlich, M. Kinne, R.J. Behm, Appl. Catal. B: Environ. 50 (2004) 209–218.
[18] Y.H. Kim, E.D. Park, H.C. Lee, D. Lee, K.H. Lee, Catal. Today 146 (2009) 253–259.
[19] A. Wörner, C. Friedrich, R. Tamme, Appl. Catal. A: Gen. 245 (2003) 1–14.
[20] S.Y. Chin, O.S. Alexeev, M.D. Amiridis, Appl. Catal. A: Gen. 286 (2005) 157–166.
[21] H. Wakita, T. Takeguchi, W. Ueda, J. Mol. Catal. A: Chem. 268 (2007) 139–147.
[22] Y.-F. Han, M. Kinne, R.J. Behm, Appl. Catal. B: Environ. 52 (2004) 123–134.
[23] C.-Y. Huang, Y.-Y. Chen, C.-C. Su, C.-F. Hsu, J. Power Sources 174 (2007) 294–301.
[24] G. Xu, Z.-G. Zhang, J. Power Sources 157 (2006) 64–77.
[25] Y.-F. Han, M.J. Kahlich, M. Kinne, R.J. Behm, Phys. Chem. Chem. Phys. 4 (2002) 389–397.
[26] M. Echigo, T. Tabata, Appl. Catal. A: Gen. 251 (2003) 157–166.
[27] M. Echigo, T. Tabata, Catal. Lett. 98 (2004) 37–42.
[28] M. Echigo, N. Shinke, S. Takami, S. Higashiguchi, K. Hirai, T. Tabata, Catal. Today 84 (2003) 209–215.
[29] M. Echigo, T. Tabata, J. Chem. Eng. Jpn. 37 (2004) 558–562.
[30] M. Echigo, T. Tabata, Catal. Today 90 (2004) 269–275.
[31] M. Echigo, T. Tabata, Top. Catal. 52 (2009) 739–742.
[32] I. Rosso, M. Antonini, C. Galletti, G. Saracco, V. Specchia, Top. Catal. 30/31 (2004) 475–480.
[33] Y.H. Kim, E.D. Park, H.C. Lee, D. Lee, Appl. Catal. A: Gen. 366 (2009) 363–369.
[34] M. Kagawa, U.S. Patent No. 7,345,007 (2008).
[35] D.F. Bakker, M.J.F.M. Verhaak, P.J.D. Wild, U.S. Patent No. 6,673,327 B1 (2004).
[36] V.P. Londhe, V.S. Kamble, N.M. Gupta, J. Mol. Catal. A: Chem. 121 (1997) 33–44.
[37] S. Takenaka, T. Shimizu, K. Otsuka, Int. J. Hydrogen Energy 29 (2004) 1065–1073.
[38] R.A. Dagle, Y. Wang, G.-G. Xia, J.J. Strohm, J. Holladay, D.R. Palo, Appl. Catal. A: Gen. 326 (2007) 213–218.
[39] M. Krämer, M. Duisberg, K. Stöwe, W.F. Maier, J. Catal. 251 (2007) 410–422.
[40] P. Panagiotopoulou, D.I. Kondarides, X.E. Verykios, Appl. Catal. A: Gen. 344 (2008) 45–54.
[41] P. Panagiotopoulou, D.I. Kondarides, X.E. Verykios, Appl. Catal. B: Environ. 88 (2009) 470–478.
[42] C. Galletti, S. Specchia, G. Saracco, V. Speechia, Chem. Eng. Sci. 65 (2010) 590–596.
[43] E.V. Kul'ko, A.S. Ivanova, G.S. Litvak, G.N. Kryukova, S.V. Tsybulya, Kinet. Catal. 45 (2004) 714–721.
[44] H.C. Stumpf, A.S. Russell, J.W. Newsome, C.M. Tucker, Ind. Eng. Chem. 42 (1950) 1398–1403.
[45] B.C. Lippens, B.G. Linsen, J.H. De Boer, J. Catal. 3 (1964) 32–37.
[46] L. Ji, J. Lin, H.C. Zeng, Chem. Mater. 13 (2001) 2403–2412.
[47] G.R. Tauszik, G. Leofanti, S. Galvagno, J. Mol. Catal. 25 (1984) 357–366.
[48] J.-L. Bi, Y.-Y. Hong, C.-C. Lee, C.-T. Yeh, C.-B. Wang, Catal. Today 129 (2007) 322–329.
[49] B. Coq, E. Crabb, M. Warawdekar, G.C. Bond, J.C. Slaa, S. Galvagno, L. Mercadante, J.G. Ruiz, M.C.S. Sierra, J. Mol. Catal. 92 (1994) 107–121.
[50] P. Betancourt, A. Rives, R. Hubaut, C.E. Scott, J. Goldwasser, Appl. Catal. A: Gen. 170 (1998) 307–314.
[51] H. Madhavaram, H. Idriss, S. Wendt, Y.D. Kim, M. Knapp, H. Over, J. Aßmann, E. Löffler, M. Muhler, J. Catal. 202 (2001) 296–307.
[52] I. Balint, A. Miyazaki, K. Aika, J. Catal. 220 (2003) 74–83.
[53] J. Assmann, V. Narkhede, L. Khodeir, E. Lffler, O. Hinrichsen, A. Birkner, H. Over, M. Muhler, J. Phys. Chem. B 108 (2004) 14634–14642.